Published in: Understanding Atrial Fibrillation: the Signal Processing Contribution
(S. Cerutti, L. T. Mainardi, L. Sornmo, eds.), ch. 7, pp. 151-173,
Synthesis Lectures on Biomedical Engineering, Morgan & Claypool (2008)
http://dx.doi.org/10.2200/S00153ED1V01Y200809BME025

Modeling AF: from myocardial cells to ECG

Adriaan van Oosterom, Vincent Jacquemet
Department of Cardiology, Centre Hospitalier Universitaire Vaudois (CHUV),
CH-1011 Lausanne, Switzerland

September 10, 2007

1 Introduction

The standard 12-lead ECG is the most commonly used non-invasive tool for diagnosing cardiac electrically manifest abnormalities like those of arrhythmias. It presents simultaneously recorded electric signals, derived from nine electrodes placed on the thorax and the extremities. The wave forms of the signals are lead specific. An example of an ECG (lead V1), recorded during a normal heart rhythm, is shown in the upper trace of Fig. 1. The PQRSTU nomenclature indicated was introduced by Einthoven [1]. In contrast, the middle trace of Fig. 1 shows the typical wave form observed in the lead V1 in a patient during atrial fibrillation (AF). Here the atrial activity is continuous, producing signals with irregular wave forms that are superimposed on the ventricular signals. The ventricular heart rate is more irregular than during sinus rhythm. However, it is less irregular than the fibrillating atrium owing to the fact that the electric trigger from atrial to ventricular tissue passes through, and is regulated by the specialized cells of the atrio-ventricular(AV) node. The atrial signals are clearly much smaller, roughly 10 times, than those related to the ventricles (QRST complexes), both during normal rhythm (P waves) and arrhythmias like AF. As a consequence, the early diagnostic applications of the P wave forms were necessarily limited, and the use of the ECG during AF was mainly restricted to diagnosing the presence of AF as such.

Besides using the ECG signals, the electrical activity of the atria is recorded by passing catheter-guided electrodes through one of the major veins into the atria. The analysis of the recorded signals (endocardial electrograms), with their far greater temporal detail, is used in diagnostic procedures as well as for guiding therapeutic interventions [3]. Advanced mapping procedures have been developed for scanning the electric activity on the exposed atrial surface [4] or endocardium [5]. Recent developments include the application of such methods in devices such as Carto and Ensite. In the Carto method, subsequent single lead recordings of the potential are taken at different locations on the endocardium, while at the same time building up a geometric representation of the atrial surface from the electrode locations, which sample 3D space. The Ensite method involves the simultaneous sampling of the potentials at a regular grid placed within the atria. The endocardial potential field and signals are derived from a computational inverse procedure. At present the Carto method does not provide simultaneous recordings and, hence, the application to arrhythmia is limited. The inverse procedure involved in processing of the simultaneous recordings used by the Ensite device has only a limited accuracy. Such methods have led to the identification of different types of foci that may trigger AF, the description of their specific dynamics and their location.

In contrast to a catheterization procedure the recording of conventional ECGs from the thorax is non-invasive. The ECG provides a global, overall impression of the atrial activity, an impression that catheterization provides only through an elaborate, time consuming procedure. However, when relying on body surface potential, an unfortunate consequence of the spreading out of electric current is that the electrical image that appears on the body surface is blurred: spatial and temporal definition is less than that of potentials observed on the atria. Their amplitudes are about 10 times smaller than those recorded by means of catheters.

Current basic research is aimed at linking the epi- or endocardial signals with different etiologies of the disease. In view of an ultimate application of the insight gained in clinical diagnostic procedures it is of interest to study how much of the spatiotemporal complexity observed at the atria might be retained in signals observed on the body surface.

The development of signal processing tools aimed at isolating the contribution of the atria to the ECG signals during AF (Chapter 2) have opened up a

clear view on these signals (lower trace of Fig. 1). This opens the way to the full extraction of the spatiotemporal information of AF signals and has strengthened the motivation for studying the diagnostic potential of body surface signals.

This chapter describes a biophysical model of the electric sources of the atria during AF, derived from membrane kinetics. In addition, it is shown how the transfer between electric sources and resulting potentials may be computed by using a volume conductor. The combination of both models can be used to study the amplitudes and waveforms of signals as observed invasively as well as on the thorax. The model based approach permits the study of atrial signals on the body surface that are completely free of contamination by ventricular electric activity. Examples of some early applications of this model-based approach can be found in [6].

2 Genesis of electrocardiographic potentials: the forward problem

When interpreting the electric signals arising from the heart's activity invariably two separate factors are involved. The first is the specification of the (active) electric current sources. The second, equally important factor is a description of the effects of the passive electric properties of the medium surrounding the heart: the body tissues. The currents generated by the heart's active properties pass through this medium, where they set up the potential differences observed between the two terminals of any lead system used.

In their diagnostic application of observed ECG wave forms, most cardiologists (and electro-physiologists) are usually not aware of these separate factors and they perform a mental signal analysis on the observed signals based on training and past experience. However, when trying to stretch the diagnostic performance of ECG based techniques both factors need to be considered.

The computation of the electric potential field generated by cardiac electric sources is generally known as the *forward problem of electrocardiography*. In solving this problem the two factors mentioned before are handled by formulating a model of the electric cardiac sources, the *source model*, as well as of the conductive tissues surrounding these sources, the *volume conduction model*. Due to the complexity of living tissue, morphology as well as function-wise, a

full description of these factors is beyond reach. Instead, different models have been postulated for handling both factors, with their complexity tuned to the particular application in hand. The models discussed in this chapter aim at providing a description of the genesis of atrial signals that does justice to the physical and electrophysiological complexity involved. A more complete treatment of the forward problem can be found in several excellent textbooks, such as[7–9].

The models used in our current work as well as their background are summarized in the following two sections.

3 Source Models

The single current dipole is probably the best-known model of the cardiac electrical generator. It is the basis of vectorcardiography (VCG). In Einthoven's papers as well as in his correspondence with Lewis and Wilson [10] it can be seen as an arrow drawn on a plane, representing the electromotive force of the heart.

However, the dipole cannot be interpreted directly in terms of the underlying electrophysiology, and certainly not for modeling, in a forward sense the electrophysiological complexity of AF. It is for this application that the source model described below holds more promise.

3.1 Electrophysiological background

The contractile elements of the atria are located inside the myocytes, a structure of densely packed cells that form a muscle layer. The overall geometry of the atrial model used is shown in Fig. 2. The hull shown, containing the myocytes, forms a *closed* surface in the sense that any of its interior points may be connected to any other interior point while following a route that lies entirely within the hull.

The activation and de-activation process of the contractile elements is controlled by calcium ions (Ca^{2+}), the intracellular concentration of which is gated by the instantaneous potential difference across the cell membrane, the transmembrane potential (TMP): $V_{\mathrm{m}}(t)$, the potential of the intra-cellular region minus that of the extracellular medium just outside the cell membrane. This

potential $difference$ depends on the concentrations of various other ions, in particular the sodium (Na^+) and potassium (K^+) ions. These "gatekeepers" of the associated fluxes of ions across the membrane are localized in the cell membrane. They are the so-called ion channels, for which several different, ion-specific variants have been identified. The entire process of activation and recovery arises from the complex, dynamic interplay between these ions, fed by the underlying biochemical processes that supply the required contractile energy.

At the end of the atrial diastolic interval all transmembrane potential levels are close to their resting state: a polarized state with an interior potential of about -80 mV. Following an initiating stimulus, the transmembrane potential rises rapidly to a level level of about +5 mV, a polarity reversal generally called *depolarization*, facilitating the activation of the contractile elements. Once a sufficiently large region is active, the polarized myocytes at the border of the activated region are depolarized by an electric current flow from the activated region. In turn, their activation facilitates that of any neighbors still at rest. In this manner, a wave-like activation process is set up. Following activation, the myocytes gradually return to their resting state. During the first part of this recovery phase, the so-called refractory period, re-activation is impossible.

In a normal heart, the initiation of the activity stems from a structure of specialized cells, the so-called sino-atrial node (SAN), which is located in the right atrium close to the superior vena cava (Fig. 2). From there the activation propagates in a regular fashion over the atrial tissue at a velocity of about 1 m/s. After recovery, the activation process is repeated only after a re-initiation in the SAN region.

In contrast, during atrial fibrillation parts of the myocardium are reactivated continuously by wave fronts previously set up in the tissue. This requires the incoming wave front to arrive later than the local refractory period, a condition that is facilitated by any delay of the incoming wave front or by any reduction of the local refractory period. The complex geometry of the atria (Fig. 2) provides various possibilities for the formation of self-perpetuating processes around the orifices of the connecting vessels and those of the valves connnecting atria and ventricles. The condition where a wave front continuously circulates around such orifices, setting up a periodic, but highly abnormal, activation pattern at an unusually high rate, is called atrial flutter (AFL).

3.2 The Equivalent Double Layer (EDL)

During the activation and repolarization of the myocytes, electric currents flow from the interior of an activated cell to those of its direct neighbors, passing through the intercalated disks. The return currents $I_{\mathrm{m}}(t)$ that flow across the cellular membrane set up the potential field in the surrounding extracellular medium. These currents form the sources of observed electrograms (EGMs) and ECGs. By convention, a local outflow current $I_{\mathrm{m}}(t)$ (of positive charge) is attributed a positive sign.

As described by Plonsey [11], a fundamental aspect of setting up a quantitative source description of the potentials at some distance from the active membrane is that these may (indeed) be described as *current* sources, and this in spite of the fact that their strength is derived from differences between the transmembrane *potentials* of neighboring cells.

The current source strength can be derived from the transmembrane potential by applying the bi-domain theory [8, 12], which treats the myocardium as a macroscopic, homogenized medium. It uses a specification of an observation point in the intracellular and the extracellular medium by means of one and the same variable, $\vec{r}$. In its mono-domain approximation it is formulated as

$$I_{\mathrm{m}}(\vec{r},t) = \nabla \cdot \sigma_{\mathrm{i}}(\vec{r}) \nabla V_{\mathrm{m}}(\vec{r},t) \approx \sigma_{\mathrm{i}} \nabla^2 V_{\mathrm{m}}(\vec{r},t), \tag{1}$$

where $I_{\mathrm{m}}(\vec{r},t)$ is an impressed current source volume density (unit: A m^{-3}), σ_{i} the electric conductivity of the intracellular domain, and $V_{\mathrm{m}}(\vec{r},t)$ the local transmembrane potential. ∇ denotes the vector operator for finding spatial derivatives (the gradient), ∇^2 the Laplacian operator (computing the divergence of the gradient). The approximation shown assumes the electric conductivity of the intracellular domain to be uniform.

A highly significant consequence of this expression is that it shows that, at all moments in time, the current sources are related to the the second spatial derivative of the transmembrane potential, $\nabla^2 V_{\mathrm{m}}(\vec{r},t)$, rather than to the transmembrane potential *per se*. This means that no external potential fields are generated by the activity at location $\vec{r}$ if $\nabla V_{\mathrm{m}}^2(\vec{r},t)$ is zero, or more generally, if $\nabla \cdot \sigma_{\mathrm{i}}(\vec{r}) \nabla V_{\mathrm{m}}(\vec{r},t)$ is zero. In case all myocytes are uniformly polarized the external field is zero. This is the condition usually assumed to prevail at the end of repolarization.

In the extracellular medium, taken here for the present moment to be of infinite size, with electric conductivity σ_{e}, the potential $\Phi(\vec{y},t)$ as generated by I_{m} as in (1) follows from solving the differential equation [13]

$$\sigma_{\mathrm{e}}\nabla^2\ \Phi(\vec{y},t) = I_{\mathrm{m}}(\vec{x},t), \tag{2}$$

which expresses the conservation of current. For reasons of clarity, $\vec{y}$ and $\vec{x}$ are used to denote the position of the field point and the source location, respectively. In the bi-domain approach, for any point inside the myocardial wall we have: $\vec{y} = \vec{x} = \vec{r}$. For a field point outside the myocardium, with no so-called primary sources present, we have

$$\sigma_o\nabla^2\ \Phi(\vec{y},t) = 0, \tag{3}$$

with σ_o the conductivity of the medium outside the heart.

A conceptually important first step in finding the potential field resulting from the current source is the computation of the so-called infinite medium potential. This is the potential field in the extracellular domain generated by the sources when placed inside a medium having an infinite extent and a homogeneous conductivity. When taking $\sigma_0 = \sigma_e$, the infinite medium potential solution to Eqs. (2) and (3), after substitution of Eq. (1), is

$$\Phi_\infty(\vec{y},t) = \frac{\sigma_{\mathrm{i}}}{4\pi\sigma_e}\int_{\mathrm{V}}\frac{\nabla^2 V_{\mathrm{m}}(\vec{x},t)}{r}\ \mathrm{d}v, \tag{4}$$

with r the length of the vector $\vec{r}$ from any source location source $\vec{x}$ to field point $\vec{y}$. The volume integral in (4) is taken over all active sources within the entire atrial myocardium.

In spite of its simplicity, equation (4) is not very practical when computing the potential fields arising from a source distribution in 3D space (the myocardium). The following, alternative expression was formulated by Geselowitz, [13, 14], who derived it by applying some classic results from field theory. It reads

$$\Phi_\infty(\vec{y},t) = \frac{-\sigma_{\mathrm{i}}}{4\pi\sigma_e}\int_S V_{\mathrm{m}}(\vec{x},t)\ \mathrm{d}\omega, \tag{5}$$

with $\mathrm{d}\omega = \mathrm{d}\omega(\vec{y}, \vec{x})$ the solid angle subtended at field point $\vec{y}$ by an element around point $\vec{x}$ of the closed surface S bounding all atrial myocytes (endocardium and epicardium) .

Expression (5) shows that the integration over 3D space involved in (4) may be replaced by an integration over the bounding surface S, which has significant conceptual as well as computational advantages. The expression holds true for the mono-domain approximation, provided the intracellular conductivity σ_{i} is taken to be uniform. No reliable experimental values of σ_{i} are currently available to permit a meaningful evaluation of the consequences of non-uniform tissue properties.

The nature of (5) permits the identification of an equivalent double layer current source (EDL), located at S, with strength $\sigma_{\mathrm{i}} V_{\mathrm{m}}$. Its strength is expressed in units A/m=Am/m^2, which reveals its nature: a current dipole density per unit surface area.

The application of this source model requires the specification of the surface S as well as of the transmembrane potential at this surface.

4 The Volume Conductor Model

The potential field generated inside the thorax and on its surface by myocardial sources is influenced by the electric conductivities of the surrounding tissues. The latter are commonly modeled by non-intersecting compartments, each having a specific, homogeneous conductivity.

The effects of inhomogeneity can be computed by different methods. In our work we use the boundary element method (BEM)[8, 15, 16]. This method computes the potential distribution throughout the body from

$$\Phi(\vec{r'}) = \frac{\sigma_s}{\sigma}\Phi_\infty(\vec{r'}) - \frac{1}{4\pi\sigma}\sum_\ell(\sigma_\ell^- - \sigma_\ell^+)\int_{S_\ell}\Phi_l(\vec{r})\frac{\vec{R}\cdot d\vec{S}}{R^3}, \tag{6}$$

with

$\Phi_\infty(\vec{r'})$ the infinite medium potential, as, *e.g.*, in (5),
σ_s the conductivity of the source region,
S_ℓ the interface bounding compartment l,
σ_ℓ^+ the conductivity just outside S_ℓ ($\ell = 1, N_S$) the number of interfaces,

σ_ℓ^-	the conductivity just inside S_ℓ,
σ	the conductivity at $\vec{r'}$, the observation point,
$\vec{r}$	a point at the interface S_ℓ,
$\vec{R}$	$=\vec{r'} - \vec{r}$; of length R.

Equation (6) constitutes the essence of the BEM. It expresses the potential field in the "real world" medium as the potential inside a virtual infinite medium generated by the impressed primary sources (expressed by the first term on the right in (6)) and of virtual double layer sources at each of the interfaces bounding the sub-regions (second terms on the right). Note that the contributions of these secondary sources on any interface may be neglected if the difference between the conductivity values at both sides of the interface is small.

The major inhomogeneity involved is the torso boundary, where the conductivity drops to zero in the exterior region (air). Other major inhomogeneities that have been identified are those of the lungs and those resulting from the blood inside the ventricular and atrial cavities. The conductivity values of these compartments, relative to the mean conductivity value of the thorax, are 1/5 and 3, respectively. The geometry of these major compartments is shown in Fig. 3.

4.1 Potentials at arbitrary field points

In practical applications to arbitrary field points, (6) can only be used if the potentials at the interfaces are known. These are computed by taking first the nodes at all interfaces as field points. The numerical implementation of this leads, for each of a set of N observation points placed on the interfaces, to a linear equation in the $n = 1, 2 \ldots N$ unknown potentials. The total set of N equations in the N unknown values is solved by computer implementations of the appropriate methods of linear algebra.

The solution found is unique only up to a constant, corresponding to the nature of the physics of the problem: the gradient of the potential at the body surface is zero. This requires the specification of a point inside the medium, or on its boundary, to act as a potential reference. In this way a unique solution is specified, in the same manner as carried out while measuring bioelectric potentials. The reference point may be chosen at will. As shown in [17, 18], there is

no natural, theoretical optimum location for the potential reference. The reference used in all examples shown in this chapter is the Wilson Central Terminal (WCT). This is an artificial reference, commonly used in electrocardiography, formed by averaging the potentials at both arms and the left foot.

The outcome of the entire procedure for determining all elements of a N-dimensional numerical vector may be formulated as a multiplication of the (numerical) vector of infinite medium potentials at arbitrary field points by a transfer matrix, say $\mathbf{A}$. The latter constitutes a numerically determined set of weighting coefficients, representing the effect of all volume conductor effects, i.e., the bounds of the volume conductor and its internal inhomogeneities. In this manner both body surface potentials (ECGs) and anywhere inside the thorax (EGMs) can be computed.

4.2 A general forward formulation

Both the source description and the volume conduction effects as discussed above may be expressed by means of matrices: the sources by a matrix $\mathbf{S}$, whose elements $s_{n,t}$ express the EDL source strength of node n of the atrial surface at time instant t, and a transfer matrix $\mathbf{A}$ with $a_{l,n}$ the potential generated at observation point l (electrode position) by a unit strength source element at node n:

$$\boldsymbol{\Phi} = \boldsymbol{AS}. \tag{7}$$

Recall that the EDL source strength on the surface S is proportional to the local transmembrane potential, (5).

The boundary element method permits the computation of the potentials at any observation point inside the thorax. Observation points on the atrial surface result in EGMs; those on the torso surface result in ECGs.

5 Modeling activation and recovery

As described in Sect. 3.1, the electric forces driving the activation process are situated in, or near, the cell membrane. The EDL source description of atrial potentials (5), as summarized in Sect. 3.2, requires the specification of the transmembrane potential at the surface S bounding the myocardium. These in turn stem from the sequence of depolarization and repolarization of the myocytes.

For modeling the activation sequence of the atria following the initiation at the SAN, a simplified approach based on the general principle of propagation following the Huygens principle has been shown to yield a surprisingly realistic[19] and useful[20] results. However for a description of the propagation and recovery during AF, the complexity involved demands a detailed description of the ion kinetic taking place at the cell membrane. This method is briefly summarized below.

5.1 Propagation derived from membrane kinetics

The activation and recovery processes of the myocytes depend on the properties of the membrane channel kinetics as well as on the way in which the individual cells are electrically coupled to their direct neighbors. Morphological studies have yielded detailed information about cell coupling.

Mathematical modeling of the membrane kinetics has produced wave forms of transmembrane potentials of single cells that closely resemble those observed experimentally. For human atrial myocytes the most commonly used description of the ion kinetics is the model postulated by Courtemanche, Ramirez and Natel (the CRN model) [21]. It takes into account the instantaneous concentration of 12 different types of ionic channels, the variations in Ca^{2+}, Na^{+} and K^{+} intracellular concentrations, and the calcium dynamics in the sarcoplasmic reticulum. This is the kinetics model involved in the results described in this chapter.

The computation of $V_{\mathrm{m}}(t)$ and $I_{\mathrm{ion}}(t)$ for a single cell involves solving a system of 21 coupled non-linear differential equations [21], for which standard numerical methods are available.

Based on a specification of the spatial distribution of the myocytes and their coupling, the propagation may then be computed by solving the partial differential equation

$$C_{\mathrm{m}} \frac{\partial V_{\mathrm{m}}(\vec{r},t)}{\partial t} = S_{\mathrm{v}}^{-1} \ \nabla \cdot \sigma \, \nabla V_{\mathrm{m}(\vec{r},t)} + I_{\mathrm{stim}}(\vec{r},t) - I_{\mathrm{ion}}(\vec{r},t), \tag{8}$$

where $V_{\mathrm{m}}(\vec{r},t)$ denotes the transmembrane potential at location $\vec{r}$ at time t, C_{m} the membrane capacitance (unit: F m^{-2}), S_{v} the cell surface-to-volume ratio (unit: m^{-1}), σ the electric conductivity of the medium (unit: S m^{-1}). The

surface-to-volume ratio S_{v} represents the total area of cell membrane per unit of tissue volume.

The system is driven by the ionic current density $I_{\mathrm{ion}}(\vec{r}, t)$ (unit: A m^{-2}) generated by the active processes near the membranes and are computed by solving, for each cell considered, the CRN kinetics equations. Any external stimulus activating the tissues is represented by the impressed current density $I_{\mathrm{stim}}(\vec{r}, t)$ (unit: A m^{-2}).

Equation (8) constitutes a so-called reaction diffusion equation. The term $S_{\mathrm{v}}^{-1}\ \nabla \cdot \sigma \nabla V_{\mathrm{m}}(\vec{r}, t)$, the diffusion term, represents the electric current flowing into the cell as a result of the intercellular coupling between neighboring cells and their potential differences. Formulation (8) is expressed in the so-called monodomain approximation of the bi-domain formulation governing the propagation of the cardiac impulse in the myocardium [8, 12].

5.2 Units representing the myocardial cells

Equation (8) is expressed in continuous variables of space and time. The numerical handling of this expression demands the introduction of a spatial discretization. This is carried out by introducing so-called *units*, each representing the activity of a conglomerate of myocytes. The large number of myocytes involved in any tissue model, for the atria alone as many as $\approx 2 \times 10^8$, the different types of ions, ion-channels and their numerous gating parameters, prohibit the formulation of a fully comprehensive number of units. The computer models of electrical propagation in the atria [22–28] differ in their representation of electrophysiological and atrial anatomical details. Typically, rather than dealing with the $\approx 2 \times 10^8$ myocytes of the atria, a far smaller number of coupled *units* have been used in this type of research, as many as 4,000,000 in some of these.

Propagation of activation relies on the interaction of neighboring myocytes and/or specialized cells like those in the SAN region and those of the atrioventricular node. Different types of mathematical methods have been worked out for simulating normal propagation processes as well as for studying the conditions that give rise to fibrillatory, chaotic-like behavior of the entire system.

6 Model parameters as used in the examples

The specifications of the model and its parameters used in the examples presented in the subsequent sections are as follows.

The geometry involved was from magnetic resonance (MR) images of healthy subjects. Details of the collection and basic processing of these data are included the cited references to earlier publications.

In addition to the introductory treatment in the previous sections, this section specifies some of the details of the models used in the simulation of the various signals shown in the final section.

6.1 Atrial model

The atrial model was derived from data first published in form a mono layer [27]. Its geometry was specified by about 100,000 nodes. Subsequently, based on this mono layer, a thick-wall variant was constructed, having a wall thickness in the range of 1.2–1.5 mm. The boundary was represented by a triangulated surface, specified by 1297 nodes. Within the resulting, closed hull bounding the atrial myocardium, some 800,000 units were placed in a locally cubical array, with spacing of 0.3 mm [20]. Details of the geometry are indicated in Fig. 2.

6.1.1 Simulated normal propagation

Propagated activation and recovery was simulated by means of the method described in Sect. 5.1. Standard settings for the parameters of CRN membrane were taken from the literature [21] *et al.* The settings of the parameters in (8) were: $C_{\mathrm{m}} = 1\ \mu\mathrm{F/cm}^2$, $S_{\mathrm{v}} = 0.24\ \mu\mathrm{m}^{-1}$, $\sigma = 0.56$ S/m (uniform, isotropic) in the bulk of the tissue. Equation (8) was solved numerically on a cubical grid in the interior of the atrial wall, using a finite difference approach [29], with time steps ranging from 12.5 to 50, adapted to the dynamical state of the ion kinetics [30]. At the surface bounding the myocytes, the normal spatial derivative of the transmembrane potential was used as the boundary condition. Following the application of a stimulus applied in the region of the SAN, a single wave front propagated over the atrial surface at a velocity of 0.7 m/s. The activation sequence agreed qualitatively with the data reported in the literature for normal atria.

6.1.2 Substrate for AF

When using a uniform setting for all parameters of the kinetics model it was found that AF like activity could not be introduced. Following any rapid pacing, which introduced and maintained a chaotic type of atrial activation, the system invariably returned to a fully polarized when the stimulus ended. In order to create a substrate for AF some of the parameters of the CRN kinetics were modified. These were aimed at creating patchy heterogeneities (at a spatial scale of about 2 cm), affecting the the intrinsic value of the local action potential duration APD_{90}[31]. To this end the channel conductances associated with the ionic currents I_{to}, I_{CaL}, I_{Kur} and I_{Kr} were scaled with respect to those used for normal propagation. Two different sets of values were used. In set A, the above parameters were scaled with respect to the normal settings by factors 3, 0.5 , 1, and 3, respectively. These values were assigned to the major part of the tissue. For the second set, B, these scaling factors were 0.2, 0.7, 0.1, and 1.5, respectively. The values of set A were assigned to the major part of the tissue, those of set B to the patches. With these settings, when stimulated from the SAN area at a rate of 120 bpm, the APD_{90} values observed over the entire surface showed a range of 150–230 ms (mean: 195± 15 ms). For these inhomogeneous parameter settings, sustained AF was induced by rapid pacing (cycle length: 150 ms) during 11 seconds, with the stimulus applied to the appendage of the left atrium.

6.2 Thorax model

The geometry of a healthy subject was documented by MR imaging methods [32]. The MR images were used to extract the geometry of the heart, lungs and thorax boundary, as well as of the ventricular cavities. To this ventricular geometry, tested extensively in previous studies, the geometry of the atrial model (Fig. 2) was fitted, by means of translation, rotation and scaling. The atrial cavities were connected to the corresponding ventricular ones. These cavities constitute the major volume conduction inhomogeneities inside the thorax.

The electric conductivity was set at 0.2 S/m in the torso and in the myocardium, at 0.6 S/m in the blood filled cavities and at 0.04 S/m in the lungs, and was assumed to be homogeneous and isotropic inside each of the compartments [33]. Finally, the potentials at all conductivity interfaces were computed

by means of dedicated BEM software, developed during previous studies [32]. This is the geometry shown in Fig. 3.

7 Examples

Different validation studies on the model based approaches to the genesis of atrial signals have been carried out in our group. For the genesis of the normal P wave these can be found in [20], for AF, see, e.g., [6, 27]. Reports on studies in which the model has been applied include: [2, 6, 31, 34].

Below, we present some examples of applications of the model to describing the genesis of AF signals. The nature of the model permits us to carry out this analysis at the full spatiotemporal level of the problem involved. The signals illustrated are taken from one and the same episode of stable AF simulated over a period of 30 s.

7.1 Potentials on the atrial surface

7.1.1 Potential Fields

In this chapter different types of scalar fields have been implied. In Sect. 3.2 the transmembrane potential (TMP) over the atrial surface bounding the myocardium, S, was introduced, acting as the EDL source strength. An example of this distribution at an arbitrary point in time during a period of simulated AF is shown in Fig. 4a. At this particular moment, several different regions can be distinguished, relating to different stages of activation and recovery. Narrow bands of TMPs of about -35 mV can be observed, e.g. the one on the right atrium moving toward the right atrial appendix. Such narrow bands correspond to depolarization wavefronts moving toward the bordering, polarized zone. The magnitude of the jump in the TMP while moving across the wave front is about 80 mV. The more spread-out band of TMPs round -35 mV correspond to repolarization, migrating toward the depolarized zone with near zero instantaneous TMPs.

The potential field over S (encompassing epicardium and endocardium) has a different nature: rather than being a potential difference across the membranes of the local myocytes, it is the potential in the extracellular medium, referred

to the external reference used (WCT). The potential field generated by the source strength depicted in Fig. 4a is shown in panel (b) of the same figure. By comparing both panels, the major features difference observed are a reversal of the polarity of the potential gradient across the wave fronts. On the epicardium, ahead of the wave front the potentials are about 10 mV higher than behind it. On the endocardium the jump is somewhat smaller. The spatial mean of the TMP over the entire surface S varies with time (mean: -54 mV, range: -61 – -45 mV). For this time instant (as well as for all other), the spatial mean of the simulated external potential on S is zero. This relates to the fact that the spatial mean of the EDL source (5) constitutes a closed uniform double layer, which has the property of producing no external field [9, 35].

The reversal of polarity corresponds to the fact that the external potentials are generated by the return of the activating currents, that -in the intracellular domain- flow toward the region still at rest(polarized).

The differences in the potential jumps across the wave front, -80 mV, *vs.* 10 mV, can be explained on the basis of equations (5) and (6). When the wave front (in the tissue), passes the *external* observation point on S, the solid angle jumps by 2π. Inserted in (5) this would "predict" a jump of $40\frac{\sigma_i}{\sigma_e}$ mV in the external field. The order of magnitude of the 10 mV jump in the external medium may be checked by taking realistic estimates of the various conductivities, and taking into account the volume conduction effects due to the three fold higher conductivity of the blood inside the cavities, computed by using (6). These inhomogeneities also explain the smaller values of the jumps on the endocardium relative to those on the epicardium. In "real life" situations the actual scaling factors involved may also differ due to local differences in the thickness of the atrial wall.

7.1.2 Signals

Although the patterns shown in Fig. 4 are similar, they are by no means identical. In fact the spatial correlation coefficients between these fields, computed over a period of 2 s showed values ranging between -0.79 and -0.52 (mean: -0.70). This corresponds to their different nature: the TMP values shown depend, exclusively, on the *local* source strength, but those of the potential field are generated by all sources distributed over S.

These differences are immediately evident when comparing the source strength

and the external potential as a function of time. The two upper traces of Fig. 5 serve for such a comparison. The upper trace depicts the TMP at an epicardial node (node n1) indicated in Fig. 4. The middle trace shows the EGM (simulated) "recorded" directly at the same node. The potential reference is the WCT. In this EGM, the passing of a wave front below the electrode is dominated by the fast downward slope. This passage is a *local* phenomenon that is surrounded by large spatial gradients. The magnitude of the fast downward signal component is about 10 mV. The starting level of this component, the amplitude of the "R wave", and consequently also the value of the "S wave" , depend, on the more diffuse contributions of all source elements over S.

Following the passage of the wave front, some expression of local repolarization can be seen in the EGM. Since the local, spatial gradients during this stage are much smaller, the signal values are also much smaller. During AF, there is an ongoing activity of distal sources, which prevents an accurate, direct interpretation of local repolarization on the based on just a single EGM.

The signal shown in Fig. 5 might be classed an EGM taken under ideal conditions: the electrode was in direct contact with the epicardium. When the distance between sensing electrode and active tissue increases, the expression of the passing wave front gets more diffuse, the amplitudes of the signals are reduced, their interpretation more difficult.

In clinical practice, the EGM shown in Fig. 5 is in called a "unipolar" lead. This is in fact a confusing, and basically incorrect, term: the recording of any potential difference always requires at least two poles, or terminals. In addition to unipolar leads, so-called "bipolar" leads are recorded, recordings of the potential difference between two closely spaced electrodes. This electrode configuration is more sensitive to the contributions of local sources than to those of distal sources, all the more so the smaller the inter-electrode distance. As such it may be viewed as a spatial filter. Unfortunately, this filter does not just reduce the signal components generated by distal sources: in applications to the atria, e.g., those of the contaminating, ventricular sources. The filter also affects the contributions of the more local sources, both in terms of their amplitude (a reduction) and their wave form.

The model enables a comprehensive analysis of such effects. Here a single example is presented. In Fig. 6,the top panel shows the paired TMP and EGM signals at node n1, the same as the ones shown by the upper and middle traces

of Fig. 5. Below, a similar pair is shown, recorded at another node, n2, located on the epicardium of the right atrium (Fig. 4) at a distance of 1.8 cm from node n1. The lower panel Fig. 6 depicts the corresponding bipolar lead, the signal that results by subtracting the unipolar EGM at node n2 (middle panel) from the one at node n1 (upper panel). With the unipolar signals at n1 and n2 available, the interpretation of the bipolar signals is straightforward. Because of the wiring of the bi-polar lead, a fast negative deflection in the of bipolar signal corresponds to the passage of a wave front at node n1, and a fast positive deflection to the passage of a wave front at n2. If a single wave front would pass both electrodes simultaneously, the line connecting the electrodes being parallel to the wave front, the deflection in the bipolar lead will be close to zero. In this situation, the timing of local activation can not be extracted from the bipolar lead signal.

7.2 Potentials on the thorax surface

7.2.1 Potential Fields

Similar to what is shown in Fig. 4b for the atrial surface, the potentials on the thorax as generated by atrial sources during AF may be visualized in the form of maps, the body surface potential maps (BSPMs). In Fig. 7a the BSPM is shown, generated at the time instant for which the (AF) source distribution is depicted in Fig. 4a.

By comparing Fig. 7a with Fig. 4a (as well as of the potentials on the heart surface Fig. 4b, the "dramatic" influence of the volume conductor effects can be observed. The image of the source distribution on S appears in a highly diffuse, convoluted manner on the body surface.

The location of the precordial electrodes of the standard 12-lead system can be seen to signal nearly the same instantaneous potential, and as such can be seen to be sub-optimal for spatially sampling the potential field during AF.

7.3 ECG signals

The more common way of looking at body surface potentials is by means of the standard 12-lead signals. The lead V1 signal of simulated AF during the 2 s period is depicted by the lower trace of Fig. 5. The similarity between this signal

and the TMP (upper trace) of the nearest source element n1 of S is clearly " not very high". The distance between the locations of electrode V1 and n1 was was about 7 cm. Since all other (1296) source elements were located at distances of no more than 17 cm away, their simultaneously ongoing activity mingled with that of n1.

The corresponding, complete set of standard 12-lead signals is shown in Fig. 8. In this figure, rather than the limb leads AVR, AVL and AVF, the extremity leads are shown are VR, VL and VF. This un-augmented scaling puts these signals on equal footing with the precordial leads V1, $\cdots$, V6. (The augmented signals are scaled up by a factor of 1.5 as a result of the wiring of the electrodes involved, a property that was very useful in the early days of electrocardiography, when electronic amplification was not available).

Because of their chaotic background, AF signals cannot be expressed by their amplitudes. Instead, their magnitudes may be specified by the root mean square (RMS) signal values computed over some time interval. The model based approach permits the computation of the RMS values of signals simulated at any (electrode) location on the thorax. A map of these values computed from AF signals over a 2 s interval is presented in Fig. 7b. Note that the RMS values at the location of the precordial leads V1, $\cdots$, V6 are far smaller than those in the upper sternal region.

In another application of the model,the possibility of significant correlations between precordial signals, as suggested by inspection of BSPMs like the one shown in Fig. 7a, was confirmed by computing the matrix of the (estimated) linear correlation coefficients, $\hat{\rho}$, of these signals. The $\hat{\rho}$ values of neighboring leads showed values ranging from 0.75 ($\hat{\rho}$(V1,V2)) to 0.99 ($\hat{\rho}$(V5,V6)). Such highly correlated signals can not be expected to yield independent information on AF, and it suggested that the extraction of information on AF from the basis of the electrode positions of the standard 12-lead system is suboptimal. Ideally, a much denser spatial sampling of the region between the level of V1 and the upper sternal region should be used. If just the nine electrodes of the standard 12-lead system are available, an adapted electrode configuration can be applied [36].

References

[1] W. Einthoven and K. de Lint, "Ueber das normale menschliche Elektrokardiogram und die capillar-elektrometrische Untersuchung einiger Herzkranken," *Pflügers Arch ges Physiol*, vol. 80, pp. 139–160, 1900.

[2] M. Lemay, J.-M. Vesin, A. van Oosterom, V. Jacquemet, and L. Kappenberger, "Cancellation of Ventricular Activity in the ECG: Evaluation of novel and existing methods," *IEEE Trans. Biomed. Eng.*, vol. BME-53/3, pp. 542–546, 2007.

[3] V. Barbaro, P. Bartolini, G. Calcagnini, and F. Censi, "Extraction of physiological and clinical information from intra-atrial electrograms during atrial fibrillation: review of methods," *Ann Ist Super Sanita*, vol. 37, no. 3, pp. 319–24, 2001.

[4] K. T. Konings, C. J. Kirchhof, J. R. Smeets, H. J. Wellens, O. C. Penn, and M. A. Allessie, "High-density mapping of electrically induced atrial fibrillation in humans," *Circulation*, vol. 89, no. 4, pp. 1665–80, 1994.

[5] S. Shpun, L. Gepstein, G. Hayam, and S. A. Ben-Haim, "Guidance of radiofrequency endocardial ablation with real-time three-dimensional magnetic navigation system," *Circulation*, vol. 96, no. 6, pp. 2016–21, 1997.

[6] V. Jacquemet, A. van Oosterom, J.-M. Vesin, and L. Kappenberger, "Analysis of Electrograms During Atrial Fibrillation; a Biophysical Model Approach," *IEEE Engineering in Medicine and Biology*, vol. 25/6, pp. 79–88, 2006.

[7] R. M. Gulrajani, F. A. Roberge, and G. E. Mailloux, "The forward problem of electrocardiography," in *Comprehensive Electrocardiology*, P. W. Macfarlane and T. T. V. Lawrie, Eds. Oxford: Pergamon Press, 1989, vol. I, ch. 8, pp. 197–236.

[8] R. M. Gulrajani, *Bioelectricity and Biomagnetism.* New York: John Wiley & Sons, 1998.

[9] R. Plonsey and R. C. Barr, *Bioelectricity: A Quantitative Approach.* New York: Kluwer Academic/Plenum Press, 2000, second edition.

[10] H. A. Snellen, *Selected Papers on Electrocardiography of Willem Einthoven.* Leiden: Leiden University Press, 1977.

[11] R. Plonsey, "An Extension of the Solid Angle Formulation for an Active Cell," *Biophysical J.*, vol. 5, pp. 663–6, 1965.

[12] C. S. Henriquez and A. A. Papazoglou, "Using computer models to understand the roles of tissue structure and membrane dynamics in arrhythmogenesis," *Proc. IEEE*, vol. 84, no. 3, pp. 334–354, 1996.

[13] D. B. Geselowitz, "On the theory of the electrocardiogram," *Proc. IEEE*, vol. 77, no. 6, pp. 857–876, 1989.

[14] ——, "Description of cardiac sources in anisotropic cardiac muscle. application of bidomain model," *J Electrocardiol*, vol. 25 Suppl, pp. 65–7, 1992.

[15] R. C. Barr, M. Ramsey, and M. S. Spach, "Relating Epicardial to Body Surface Potentials by means of Transfer Coefficients based on Geometry Measurements," *IEEE Trans. Biomed. Eng.*, vol. BME-24, pp. 1–11, 1977.

[16] A. van Oosterom, "Electrocardiography," in *The Biophysics of Heart and Circulation*, J. Strackee and N. Westerhof, Eds. Bristol: Inst of Physics Publ, 1993, ch. 3, pp. 249–256.

[17] H. C. Burger, "The Zero of Potential: A Persistent Error," *Am. Heart J.*, vol. 49, pp. 581–586, 1955.

[18] D. B. Geselowitz, "The zero of potential," *IEEE Engineering in Medicine and Biology Magazine*, vol. 17, no. 1, pp. 128–132, 1998.

[19] P. van Dam and van Oosterom A., "Atrial Excitation using Uniform Propagation," *J. Cardiovasc. Electrophysiol.*, vol. 14, pp. S166–S171, 2003.

[20] A. van Oosterom and V. Jacquemet, "Genesis of the P wave: Atrial signals as generated by the equivalent double layer source model," *Europace*, vol. 37(Suppl.)S, pp. 21–29, 2005.

[21] M. Courtemanche, R. J. Ramirez, and S. Nattel, "Ionic mechanisms underlying human atrial action potential properties: insights from a mathematical model," *Am J Physiol*, vol. 275, no. 1 Pt 2, pp. H301–21, 1998.

[22] D. Harrild and C. Henriquez, "A computer model of normal conduction in the human atria," *Circ Res*, vol. 87, no. 7, pp. E25–36, 2000.

[23] C. J. Kafer, "Internodal pathways in the human atria: a model study," *Comput Biomed Res*, vol. 24, no. 6, pp. 549–63, 1991.

[24] E. Macchi, "Digital-computer simulation of the atrial electrical excitation cycle in man," *Adv Cardiol*, vol. 10, pp. 102–110, 1974.

[25] G. K. Moe, W. C. Rheinboldt, and J. A. Abildskov, "A computer model of atrial fibrillation," *Am Heart J*, vol. 67, pp. 200–20, 1964.

[26] E. J. Vigmond, R. Ruckdeschel, and N. Trayanova, "Reentry in a morphologically realistic atrial model," *J Cardiovasc Electrophysiol*, vol. 12, no. 9, pp. 1046–54, 2001.

[27] N. Virag, V. Jacquemet, C. S. Henriquez, S. Zozor, O. Blanc, J. M. Vesin, E. Pruvot, and L. Kappenberger, "Study of atrial arrhythmias in a computer model based on magnetic resonance images of human atria," *Chaos*, vol. 12, no. 3, pp. 754–763, 2002.

[28] C. W. Zemlin, H. Herzel, S. Y. Ho, and A. Panfilov, "A realistic and efficient model of excitation propagation in the human atria," in *Computer simulation and experimental assessment of cardiac electrophysiology*, N. Virag, O. Blanc, and L. Kappenberger, Eds. Armonk, New York: Futura Publishing, 2001, pp. 29–34.

[29] F. Fenton and A. Karma, "Vortex dynamics in three-dimensional continuous myocardium with fiber rotation: Filament instability and fibrillation," *Chaos*, vol. 8, no. 1, pp. 20–47, 1998.

[30] Z. Qu and A. Garfinkel, "An advanced algorithm for solving partial differential equation in cardiac conduction," *IEEE Trans Biomed Eng*, vol. 46, no. 9, pp. 1166–8, 1999.

[31] V. Jacquemet, N. Virag, and L. Kappenberger, "Wavelength and vulnerability to atrial fibrillation: insights from a computer model of human atria," *Europace*, vol. 7, pp. S83–92, 2005.

[32] G. Huiskamp and A. Van Oosterom, "The depolarization sequence of the human heart surface computed from measured body surface potentials," *IEEE Trans Biomed Eng*, vol. 35, no. 12, pp. 1047–58, 1988.

[33] A. van Oosterom, "Genesis of the t wave as based on an equivalent surface source model," *J Electrocardiol*, vol. 34 Suppl, pp. 217–27, 2001.

[34] A. van Oosterom, Z. Ihara, V. Jacquemet, and R. Hoekema, "Vectorcardiographic lead systems for the characterization of atrial fibrillation," *J. Electrocardiology*, vol. 40(4), p. 343, 2007, 343.el-343.el1.

[35] F. N. Wilson, A. G. Macleod, and P. S. Barker, "The Distribution of Action Currents produced by the Heart Muscle and Other Excitable Tissues immersed in Conducting Media," *J. Gen. Physiol.*, vol. 16, pp. 423–456, 1933.

[36] Z. Ihara, A. van Oosterom, V. Jacquemet, and R. Hoekema, "Adaptation of the standard 12-lead electrocardiogram system dedicated to the analysis of atrial fibrillation," *J. Electrocardiology*, vol. 40, pp. 68.el–68.08, 2007.

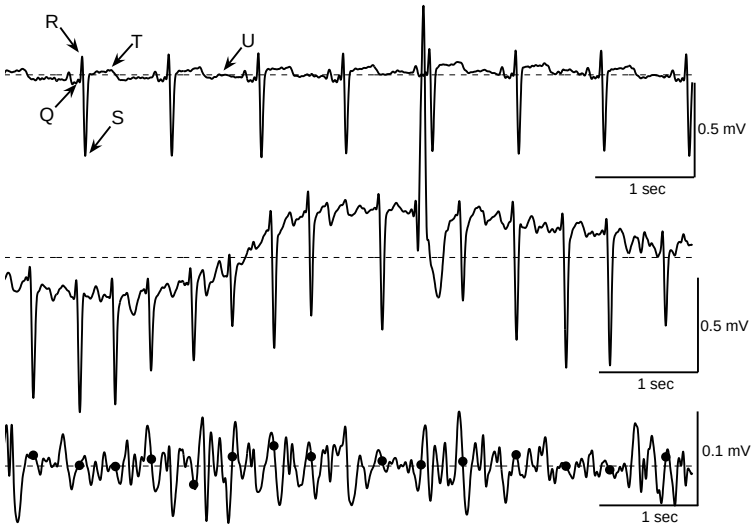

Figure 1: Wave forms of standard lead V1. Upper trace: healthy subject during sinus rhythm. Middle trace: clinical recording of AF patient; note the wandering baseline and the presence of an ectopic beat. Such beats frequently occur during AF. Lower trace: signal of the middle trace after baseline correction and suppression of the ventricular (QRST) involvement. Note its different scaling. The dots mark the timing of the S waves shown in the middle trace. ([2])

.

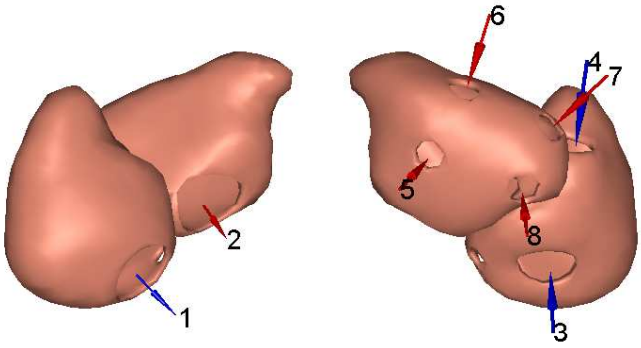

Figure 2: Atrial geometry; wall thickness approx 2 mm; Left panel: natural anterior view; Right panel: posterior view. Labels 1-8 denote the entry and exit connections of the blood to the atrial cavities: (1) mitral valve; (2) tricuspid valve; (3) inferior vena cava;(4) superior vena cava; (5) left superior pulmonary vein; (6) right superior pulmonary vein; (7) left inferior pulmonary vein; (8) right inferior pulmonary vein.

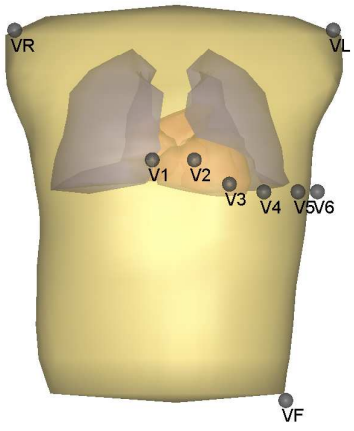

(a)

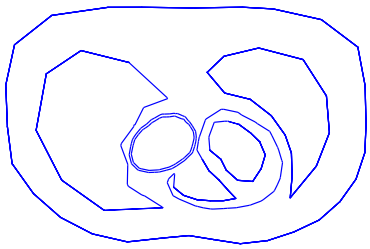

(b)

Figure 3: Panel (a): Volume conductor model. Included: thorax boundary; atria, ventricles and lungs. Geometry and locations of the nine electrodes of the standard 12-lead system, derived from MR images, are as indicated. Panel(b): transverse cross-section at the level of electrode V1. Note: (in this subject) this level does not cross the left atrium, compare Fig. 2.

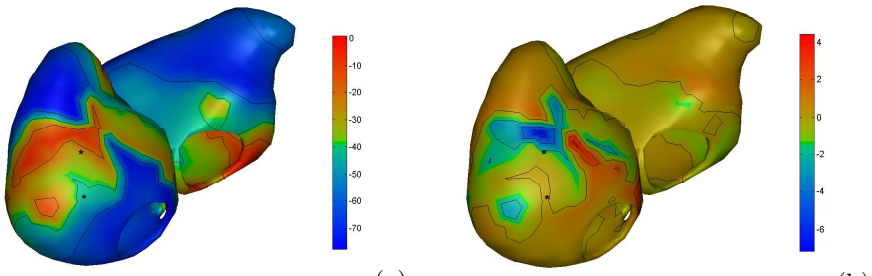

(a) (b)

Figure 4: Panel (a): Instantaneous distribution of the local TMP (the EDL source strength over the atrial surface) during AF. Anterior view of the atrial model; Isopotential line increments: 10 mV; the narrow band of potentials of about -35 mV correspond to depolarization wavefronts moving toward the bordering polarized with TMP potentials of -70 mV, the wider band to regions in which repolarization migrates toward the bordering depolarized zone zone of near zero TMPs. Panel (b) Potential distribution on the atrial surface S generated by the source distribution shown in panel(a); increments between isopotential lines: 2 mV. The lower of the two dots drawn on the right atrium mark the position of node n1, the node closest to the position of electrode V1 on the thorax, the other to a nearby node, n2, at a distance of 1.8 cm. Electrograms at these locations are shown in Fig. 6.

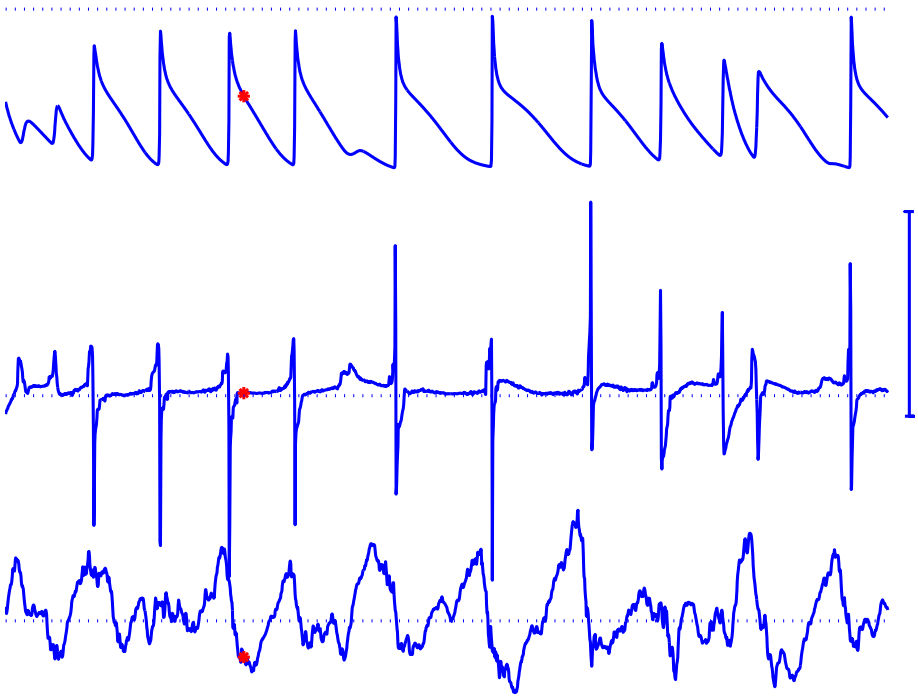

Figure 5: AF signals, simulated over a 2 s period. Upper trace: TMP at the epicardial node (node n1) of the atrial model closest to Electrode V1 on the thorax (Fig. 4. Middle trace: Electrogram at node n1. Lower trace: corresponding ECG signal of lead V1. Vertical scale corresponds to 100 mV, 10 mV and 1 mV for the TMP, the electrogram and the ECG, respectively. For all signals, the doted horizontal lines denote zero potential. The heavy dots mark the time instant for which locations the EDL source distribution is shown in the left panel of Fig. 4

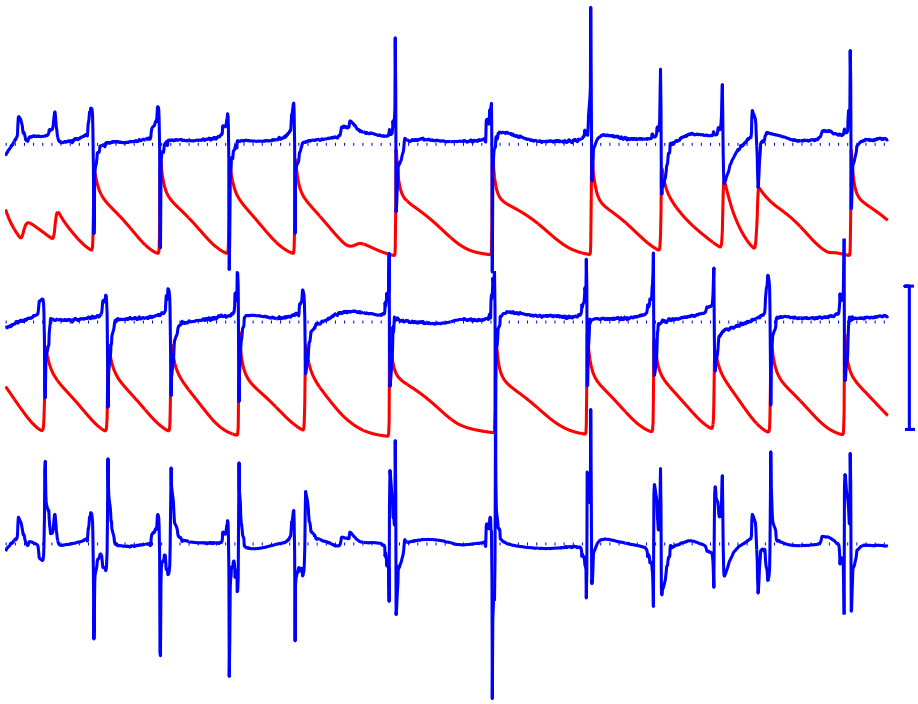

Figure 6: AF signals simulated over a 2 s period. Upper panel: superimposition of the TMP and the EGM at epicardial node n1 (Fig. 4). This pair replicates the upper two traces of Fig. 5. Middle panel: Superimposition of the TMP and the EGM at an epicardial node n2, a node at about 1.8 cm from n1. Lower panel: bipolar EGM resulting from subtracting the monopolar EGM at node n2 from that at node n1. Vertical scale as in Fig. 5.

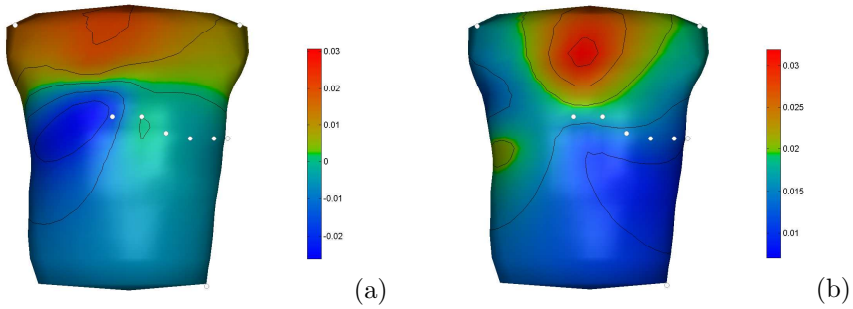

Figure 7: Panel (a): Body surface potential map generated by the EDL at the time for which source distribution is shown in Fig. 4a. Isopotential lines drawn at increments of 10 μV. Panel (b) Map of the RMS values of simulated AF, computed over a period of 2 s. Isofunction lines drawn at increments of 5 μV. Potential reference: WCT.

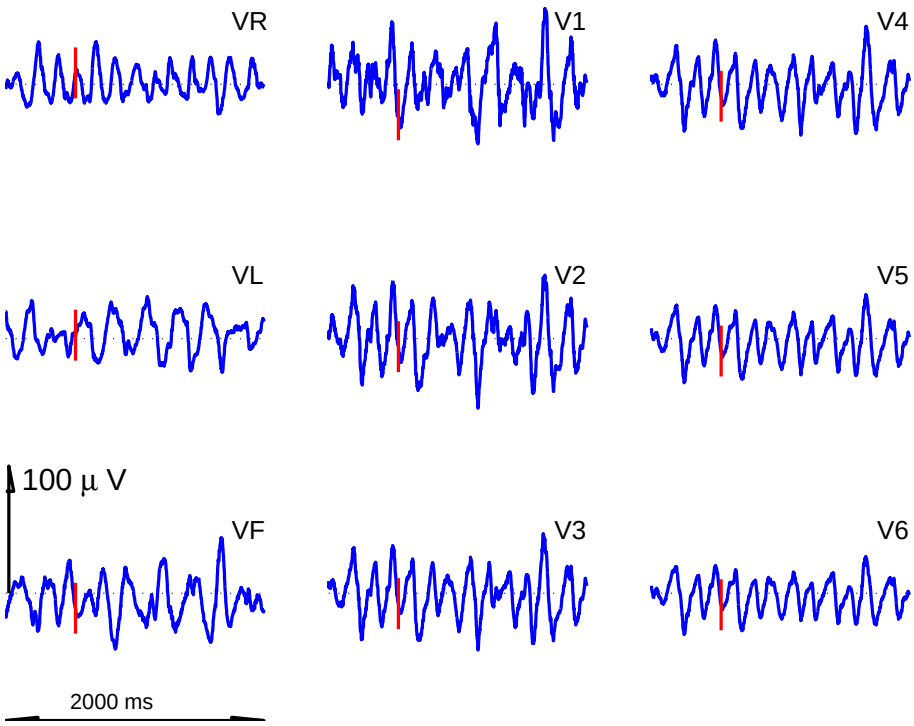

Figure 8: Standard 12-lead signals of simulated AF signals. Extremity leads VR, VL and VF un-augmented (see text). The small vertical bar shown in each signal marks the timing of the source strength shown in Fig. 4a. Time interval shown: 2 s.